Optical and Quantum Electronics (2024) 56:645
https://doi.org/10.1007/s11082-024-06294-x

# New natural dyes extracted by ultrasonic and soxhlet method: Effect on dye-sensitized solar cell photovoltaic performance

**Fehmi Aslan**[1]

Received: 22 November 2023 / Accepted: 4 January 2024 / Published online: 6 February 2024
© The Author(s) 2024

**Abstract**
This study employed soxhlet and ultrasonic methods to extract novel natural dyes from *Rhamnus tinctoria* seed, *Rubia fruticosa* fruits, and *Pinus pinea* bark, which were then used as sensitizers in dye-sensitized solar cells (DSSCs). XRD data showed that $TiO_2$ in the photoanode layer was in the anatase phase. The produced DSSCs were assessed for photovoltaic performance and electrochemical charge transfer while sensitizing dyes were characterized using UV–vis spectroscopy and FTIR. Natural dyes leached with different extraction methods showed different absorption behaviors in the UV–vis region. FTIR results revealed the presence of both carbonyl and hydroxyl groups, which enhanced the interaction between the extracted dyes and the $TiO_2$ thin film. All cells using sensitizers obtained by the Soxhlet method showed higher efficiency compared to the ultrasonic method. The highest cell performance ($\eta = 0.47\%$) was obtained with 0.71 V $V_{oc}$, 0.92 mA/cm$^2$ $J_{sc}$, and 0.72 FF for the sensitizer extracted from *Rhamnus tinctoria* seeds by the soxhlet method.

**Keywords** Dye-sensitized solar cells · Natural dyes · Dye extraction · Photovoltaic performance

## 1 Introduction

The increase in the need for energy and the rapid depletion of fossil fuels have directed many researchers to alternative and renewable energy sources (Kumar et al. 2022; Alinejad et al. 2023). Photovoltaic technology is particularly appealing among renewable energy sources because it turns sunlight directly into electrical energy (Rajkumar et al. 2019). The high cost and non-environmental nature of silicon-based solar cells have made it inevitable to develop low-cost devices (Rajkumar et al. 2022). Until now, many remarkable studies have been carried out on the production of low-cost and high-efficiency solar cells (Nnorom et al. 2022; Zatirostami 2021). Due to their low cost and

✉ Fehmi Aslan
fehmi.aslan@ozal.edu.tr

[1] Department of Motor Vehicles and Transportation Technologies, Malatya Turgut Ozal University, Malatya 44210, Turkey

ease of production, dye-sensitized solar cells (DSSCs) are very important in photovoltaic technology (Nguyen et al. 2020; Ahmad et al. 2023; Senthamarai et al. 2022). To catalyze the reaction, a typical DSSC includes a dye molecule, counter electrode, redox electrolyte, and photoanode. Dye molecules easily absorb artificial light or sunlight and excite electrons by collecting the emitted photon flux on the surface of the oxide layer. Excited electrons are injected into the metal oxide semiconductor layer's conduction band. These electrons are transferred to the current collector via the metal oxide thin film, and the dye molecule is renewed in the redox solution by an electron donor. Finally, a complete regeneration takes place by transferring electrons to the electron acceptor on the counter electrode of the DSSC (Peiris et al. 2021; Prakash et al. 2022). The working principle of a typical DSSC is given in Fig. 1. The first study on DSSCs was conducted by Gratzel et al. They have been successful in creating DSSCs with photoanodes based on titanium dioxide ($TiO_2$) that have a power conversion efficiency of more than 7% (Richhariya et al. 2022). In subsequent studies, efficiency values above 15% were achieved (Teja et al. 2023). These findings hold promise for DSSC commercialization in the future. However, more thorough research is now required because DSSC efficiency is still below the target level. Researchers have attempted to improve the dye, counter electrode, electrolyte, and photoanode of DSSCs to boost their efficiency (Sen et al. 2023).

Dye sensitizers have a great impact on the efficiency of DSSC as they greatly affects the light harvesting (Rahman et al. 2023). A typical DSSC's performance depends on the sensitizing dye's molecular structure, which separates the electron–hole pairs when excited by light. The task of the dye in DSSCs is to provide charge transfer to the semiconductor surface by converting the light into electronic excitation. The properties of a natural dye that can be used as a sensitizer in DSSCs are given below (Sánchez-García et al. 2018).

1. The dye must contain a carbonyl and/or hydroxyl group that can form a intense interaction with the semiconductor surface.
2. In the visible range, it must show strong absorption.
3. It must have a high damping coefficient.

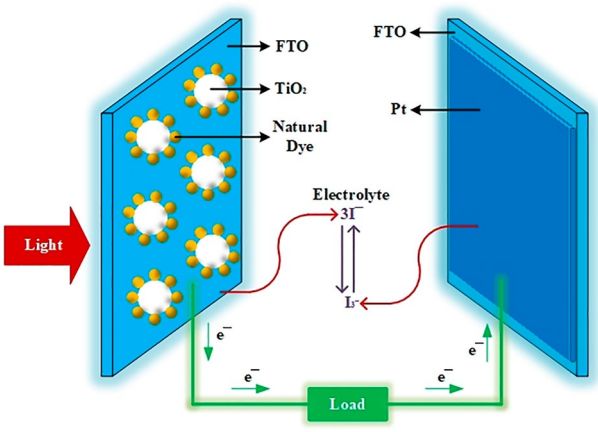



**Fig. 1** Functioning principle of a standard DSSC

4. The lowest conduction band and the LUMO level (lowest-unoccupied-molecular orbital) must line up.
5. The HOMO (level-highest-occupied molecular orbital) of the electrolyte solution to be used in DSSC must be lower than the redox level for electrons to fully transfer to the conduction band.

Many studies have been conducted on metal-based dyes that exhibit high performance on DSSCs. Metal complexes and different synthetic dye derivatives showed the highest power conversion efficiencies (Zatirostami 2020). Especially in DSSCs produced using N719 sensitizer, efficiency values over 14% were achieved. However, due to the high cost and toxic effects of such metal-based dyes, more environmentally friendly and natural dyes have been considered as alternatives. Natural plant dyes are non-toxic and can be easily synthesized at a low cost (Singh et al. 2021). However, the efficiency of DSSCs sensitized with natural dyes has not yet reached the desired level (Prakash and Janarthanan 2023). As a result, numerous research projects were carried out to raise the stability and effectiveness of DSSCs sensitized with natural dyes, using various tactics, including mixing various natural dyes (Obi et al. 2020), purification via column chromatography (Wang et al. 2006), and different extraction techniques (Calogero et al. 2015). In a study by Kristoffersen et al., a significant increase in efficiency was detected after the removal of non-pigment organic compounds from DSSCs using anthocyanin as a sensitizing dye (P. N., B. R., A.S. Kristoffersen, B. G., P. S., S. K., K. M.D., S.R. Erga, D. Velauthapillai 2021). Furthermore, an enhancement in the performance of solar cells sensitized with the betalain-anthocyanin pair was noted in the research carried out by Ramomoorthy et al. (Ramamoorthy et al. 2016). In another study by Calogero et al., the performance of DSSCs was improved by up to 1.6% by using different extraction methods to obtain sensitizing dye. (Calogero et al. 2018). Using various solvents and extraction techniques, Inbarajan et al. reported achieving a power conversion efficiency of 1.17% in another study (Inbarajan et al. 2022).

Among the dyes leached by the extraction of natural plants, the most commonly used ones are carotenoids, anthocyanins, betalains, flavonoids, and chlorophylls (Safaei-Ghomi and R.* Masoomi, M. Hosseinpour, H. Batooli 2020). The main classification of

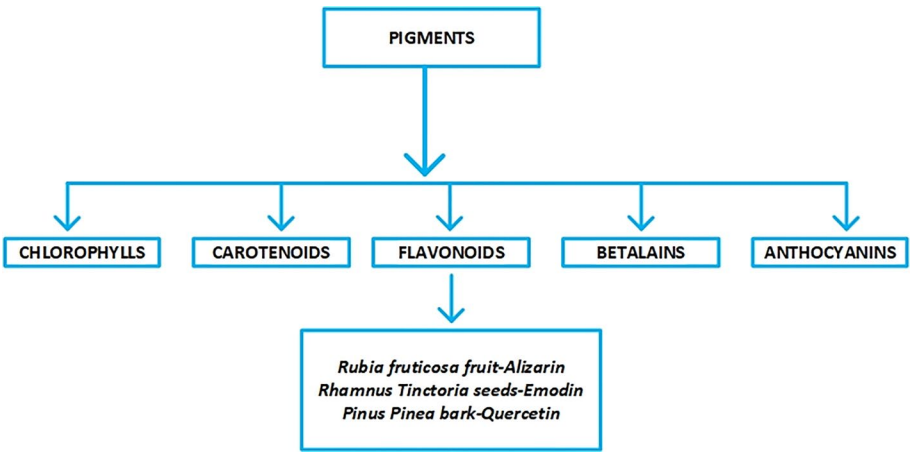



**Fig. 2** The main classification of plant pigments

plant pigments is given in Fig. 2. Plant pigmentation and chemical composition are key factors in the dye classification process. The dye's molecular makeup makes it more apt to stick to the $TiO_2$ electrode and makes it easier for electrons to flow toward the $TiO_2$ conduction band. Additionally, the dye structure helps slow charge recombination at the interface. Several chemical functional groups bind the sensitizing dye to the semiconductor metal oxide surface. Among these functional groups, there are carbonyl or/and hydroxyl groups. Dyes containing carbonyl or/and hydroxyl groups not only establish a stronger electronic connection with the photoanode but also provide a better interaction with the electrolyte solution (Tabacchi et al. 2019). Therefore, some physical and chemical properties of sensitizers used in DSSCs can significantly affect the performance of DSSCs (Kabir et al. 2022a).

Organic-based dyes extracted from natural plants are used extensively in many areas such as the textile industry, anti-viral drug research, and pharmaceuticals (Sen et al. 2023). Among these plants, *Rubia fruticosa* fruits, *Rhamnus tinctoria* seeds, and *Pinus pinea* bark are also used as dyestuffs. *Pinus pinea* bark, *Rhamnus tinctoria* seeds and *Rubia fruticosa* fruits used in this study are flavonoids (Sönmezolu et al. 2012; Gómez-Ariza et al. 2006; Espinosa et al. 2012). *Rhamnus tinctoria* is a thorny shrub plant that is up to 3 m in length and grows endemic in Central Anatolia. The seeds of this plant remain green for a long time before, they turn black and brownish. Dyes produced from the *Rhamnus tinctoria* plant were used as textile dyes from ancient times to the nineteenth century (Akin et al. 2016). Another plant species, *Rubia fruticosa*, is an endemic species that grows in the central archipelago of Macaronesia. This plant species is known for its fleshy fruits and can reach half a meter in length (Vieito et al. 2018). In addition, the *Pinus pinea* plant accounts for about 7% of the biomass above ground. It is an evergreen coniferous tree that can grow up to 30 m in height in the form of an umbrella, which is abundant in the Mediterranean basin. A brown-reddish dye is leached by extraction of the bark of this plant (Vieito et al. 2018; Agrícolas et al. xxxx). Plants contain many dyestuff compounds. The ratio of these compounds varies according to the type of plant, the region where it grows, its age, and the harvest season. The most common dyestuffs in the structure of *Rhamnus tinctoria* seeds, *Rubia fruticosa* fruits, and *Pinus pinea* bark are emodin, alizarin, and quercetin, respectively. The main classification of plant pigments used in this study can be seen in Fig. 2.

To extract maximum dye from a plant, an effective extraction is required. The factors such as economy, efficiency and ease of access play important roles in choosing the extraction method. It is also important that the chemical used in extraction has a minimum impact on the environment (Teja et al. 2023). It is known that dyes obtained by different extraction methods change the photovoltaic properties of DSSCs (Kocak et al. 2019). The most commonly used method to study the effect of the extraction method is trial and error. It is assumed that there is a strong relationship between the extraction method and the absorbance of the dye in the visible region (Mphande 2014).

Sol–gel method, Precipitation, Spray pyrolysis, Template method and Hydrothermal method are generally used in $TiO_2$ synthesis. Among these methods, the hydrothermal method creates an effective reaction environment for metal oxide production due to controllable particle size, high nanocrystallinity and high purity (Yeoh et al. 2023).

$TiO_2$ is the most widely used semiconductor metal oxide in DSSCs due to its features such as being environmentally friendly, abundant and providing the necessary surface area for good dye loading (Calogero et al. 2010; Senthamarai et al. 2021). The nanoporous $TiO_2$ layer with a large surface area coated on the conductive glass surface allows high absorption of the sensitizing dye (Weldekidan et al. 2018). The most important factor that encourages the use of $TiO_2$ in DSSCs is its ability to absorb a large portion of incoming light.

$TiO_2$ used in DSSCs is generally in the rutile or anatase phase. Anatase $TiO_2$ is used more due to its wide band gap and chemical stability (Mozaffari et al. 2015).

In this study, it was investigated to what extent dyes leached from different plant species by soxhlet and ultrasonic methods affect the performance of DSSCs. In the literature review, no studies were found on the use of dyes extracted from *Pinus pinea* bark, *Rhamnus tinctoria* seeds and *Rubia fruticosa* fruits in DSSCs. Experimental studies have shown that natural dyes obtained by different extraction methods significantly affect the photovoltaic properties of DSSCs.

## 2 Experimental

### 2.1 Materials

In this study, *Rhamnus tinctoria* seeds (Turkey-Kocaeli city), *Rubia fruticosa* fruits (Archipelagos-Canary islands) and *Pinus pinea* barks (Turkey-Izmir city) were obtained from different regions where they grow naturally. Without any purification, all of the chemicals used in the creation of DSSCs were bought commercially. Titanium-IV-isopropoxide TTIP ($\geq$97.0%:Sigma-Aldrich) and urea ($CO(NH_2)_2$, 99%, Sigma-Aldrich) were used for the synthesis of $TiO_2$ nanopowder. Ethyl cellulose (Sigma-Aldrich) and α-terpineol (Sigma-Aldrich) were chosen as binders in $TiO_2$ paste. Fluorine:doped-tin oxide (FTO, from Sigma-Aldrich) with an average surface resistivity of 13 Ω/sq was used as the conductive glass substrate. Pt-based counter electrodes were obtained from platinum pastes (Platisol T, Solaronix). Redox electrolyte (Iodolyte:AN-50, Solaronix) was used for reduction–oxidation processes and Meltonix 25 µm (Solaronix) was used as sealing material.

### 2.2 Synthesis of $TiO_2$ nanoparticles

$TiO_2$ nanoparticles prepared in this study were synthesized with the same procedure was used previously in DSSCs (Aslan 2023). The hydrothermal method was used to create the $TiO_2$ nanoparticles that were used in the photoanode layer. A homogenous structure was formed by vigorously mixing 1.6 g of urea with 40 ml of deionized water. 3.5 ml of TTIP homogeneous solution was added dropwise during this process, and it was mixed for 30 min. After 45 min of ultrasonic treatment, this mixture was placed in a Teflon autoclave to finish the hydrothermal treatment (at 120 °C for 24 h). After the hydrothermal treatment was completed, it was washed several times with alcohol and water to remove some unwanted residues from the white particles formed. Following 4 h of drying at 50 °C in the oven, the cleaned particles were calcined for 45 min at 450 °C. The particles cooled in the desiccator were converted into powder form with the help of an agate mortar and stored to prepare $TiO_2$ paste.

### 2.3 Extraction of natural dyes

Using different extraction methods, quercetin, emodin, and alizarin dyes were leached from *Pinus pinea* bark, *Rhamnus tinctoria* seeds, and *Rubia fruticosa* fruits. These plants underwent multiple washings in deionized water before being vacuum-dried for 12 h at 50 °C. The dried plant parts were converted into powder form with the help of a high-speed grinder and stored at -20 °C without exposure to light until the extraction process. In this

study, ethyl alcohol was used as a solvent in all samples to obtain sensitizing dyes, because it is known from previous studies that quercetin, alizarin and emodin dyes are more soluble in ethanol (Inbarajan et al. 2022; Shalini et al. 2015). Perez et al. reported that among the dyes they obtained from the flowers, leaves and fruits of 8 different plants using different solvents, the dyes extracted with alcohol exhibited the best performance (Ramirez-Perez et al. 2019). In the first extraction method, 10 g of each sample was weighed and placed in 3 different soxhlet cartridges and the system was allowed to siphon 5 times in a 250 ml alcohol environment. To adjust the concentration of sensitizing dyes extracted by the soxhlet method, some of the alcohol in the structure was removed with the help of a rotary evaporator. In the second extraction method, 10 g of a ground sample taken from each sample was subjected to ultrasonic treatment for approximately 1 h in beakers containing 250 ml of alcohol. The dyes produced by the ultrasonic method were adjusted to the appropriate concentration with the help of a rotary evaporator. These natural dyes were finally filtered with the help of filter paper and stored at -20 °C in the dark. The extraction processes of natural dyes are given in Fig. 3.

### 2.4 Assembling of DSSC

We took our previous work as a reference to prepare $TiO_2$ paste (Aslan 2023). In this context, 450 mg $TiO_2$, 225 mg ethyl cellulose and 1.5 ml α-terpineol were ultrasonically treated in 15 ml ethanol for 1 h. This mixture was stirred vigorously with a magnetic stirrer in a dark environment for one day. After the mixing process was completed, a certain amount of alcohol in the mixture was removed with the help of a rotary evaporator to obtain a suitable paste consistency. The produced $TiO_2$ paste was coated with a doctor blade technique on FTO conductive glasses, which were previously cleaned by the sequential ethanol-deionized water–acetone procedure. Conductive glasses coated with $TiO_2$ thin film were placed on a smooth surface and dried in an oven at 80 °C and then calcined in a muffle furnace at 450 °C for 45 min. After the calcination process was completed, the photoanodes were cooled in a desiccator to prevent oxidation. These photoanodes were dipped into pre-prepared natural dyes with the $TiO_2$ layer in the upper position and left for one day. The sensitized photoanodes were immersed several times in an alcohol solution to remove insoluble residues on the $TiO_2$ surface. Pt paste was evenly applied with acrylic brush strokes to the conductive surfaces of previously cleaned FTO glasses to create counter electrodes. The glasses were then calcined at 450 °C for 15 min. A melting gasket, also known as a sealing material, was placed around the $TiO_2$ thin films on the photoanode, and the Pt counter electrode was combined with this surface. A heat of 100 °C was applied for half a min to melt the gasket. The electrolyte solution was transferred by vacuuming the air inside with the help of a syringe through the hole on the Pt counter electrode of the sample whose electrodes were combined. Eventually, the DSSC production process was ended when the counter electrode's hole was filled with sealing material. The generated $TiO_2$ thin films were measured to have an active surface area of 0.36 $cm^2$ and a thickness of 15 µm. Figure 4 displayed a representative image of the generated DSSCs.

### 2.5 Characterization

In order to define the crystal phases being in produced $TiO_2$ nanoparticles, X-ray diffraction analysis (Rigaku Miniflex) were used in the 2θ values between 10° and 80° degree. To investigate the surface morphology of the samples, field emission electron microscopy

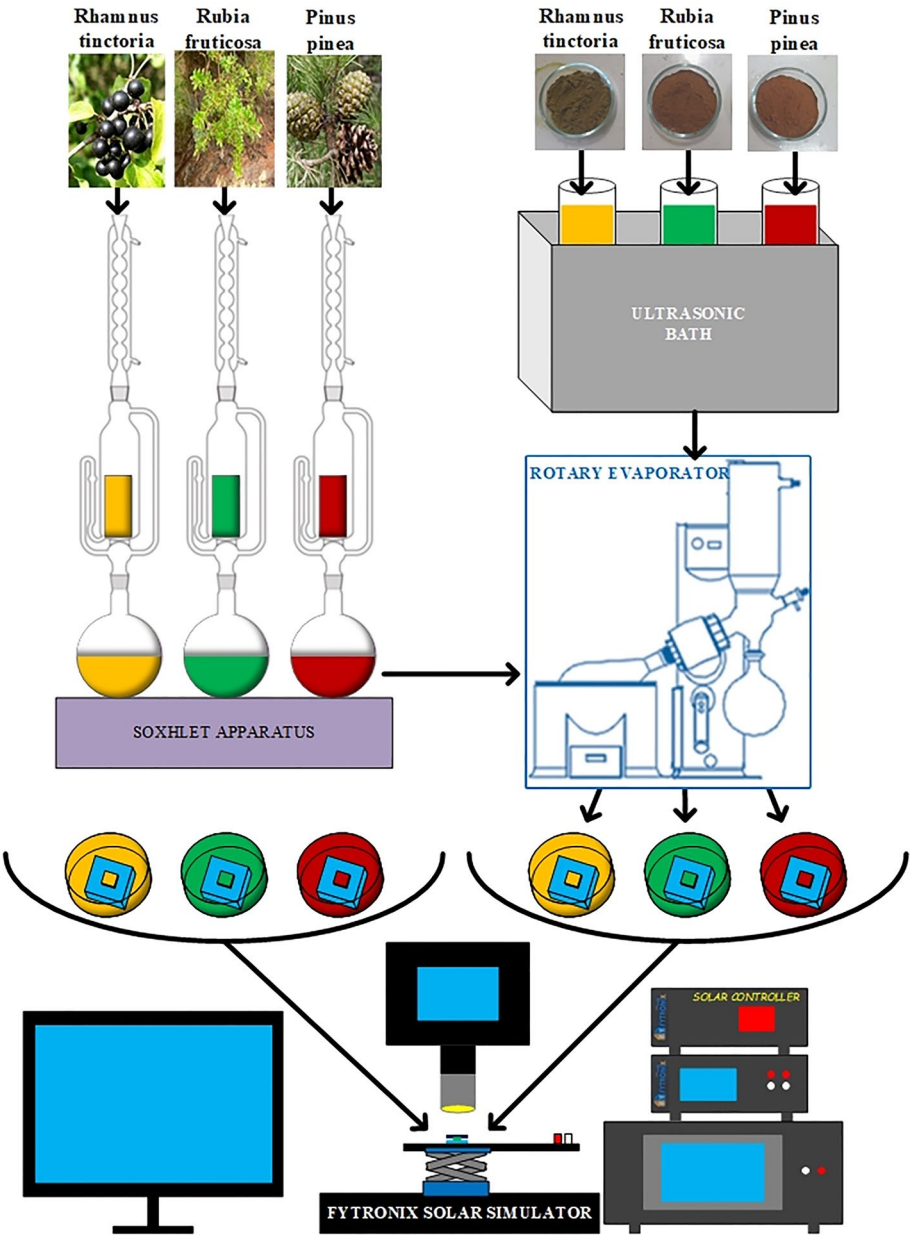



**Fig. 3** The extraction process of different natural plants

(FESEM, Zeiss Sigma) analysis was preferred. Specific surface area and pore size distribution analysis of the $TiO_2$ nanopowder were accomplished by using the $N_2$ adsorption-Bruenur-Emmet-Teller (BET, Micromeritics, ASAP 2020) isotherm method. The thickness of the thin film in the photoanode layer was measured with a profilometer (Kla Stylus Profiler P7). The UV–vis absorption characteristics of sensitizing dyes were investigated by using

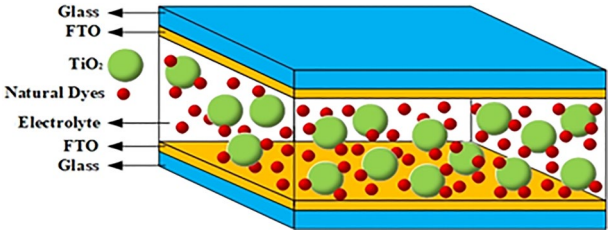



**Fig. 4** Representative view of the DSSC

Shimadzu UV-3600 spectrophotometer. The sensitizing dye samples were subjected to FTIR (Thermo Scientific, Nicolet Summit) analysis in order to determine functional groups in the structure. EIS measurements of the cells were carried out with Fy-tronix Impedance Analysis in the frequency range of 0.1–100,000 Hz and under artificial sunlight (100 mW/cm$^2$). Photovoltaic measurements of the produced DSSCs were taken with the Fy-tronix LSS 9000 solar simulator.

## 3 Results and discussion

The XRD pattern of $TiO_2$ nanoparticles produced by the hydrothermal process is shown in Fig. 5. Reflection peaks in the XRD pattern validate the anatase phase and excellent crystalline structure of $TiO_2$. Furthermore, the anatase phase and 141:I41/amd unit cell symmetry of $TiO_2$ nanoparticles match card number DB 5000223. The Williamson-Hall formula given in Eq. 1 was used to determine the average crystal sizes of the produced $TiO_2$ nanoparticles (Sethy et al. 2023).

$$\beta \cos\theta = \frac{0.9\lambda}{D} + 4\varepsilon \sin\theta \tag{1}$$

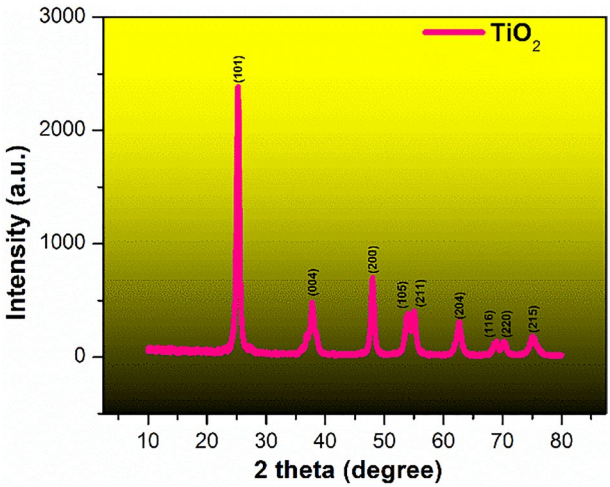



**Fig. 5** XRD diffraction pattern of produced $TiO_2$ nano powder

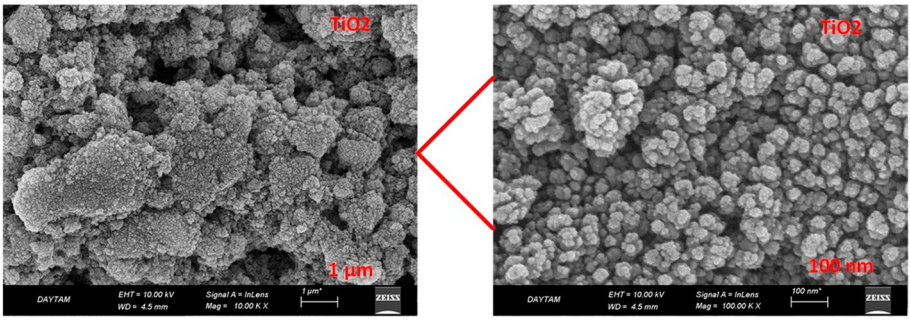



**Fig. 6** SEM images of $TiO_2$ particles at different scales

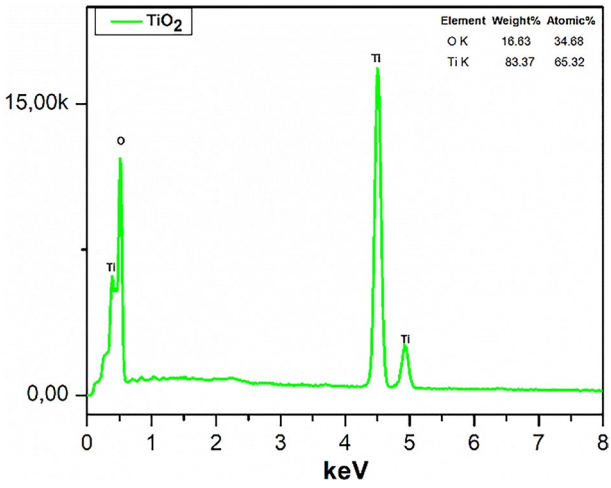



**Fig. 7** EDS analysis of $TiO_2$ particles

The symbols "λ", "ε", "D", and "θ" in this formula indicate the peak's reflection angle, crystal size, lattice strain, and X-ray wavelength, respectively. FWHM, or the full width at half the peak height, is denoted by the symbol βs. The large crystal sizes improve the photovoltaic conversion efficiency of cells. Because the increase in crystal size reduces the grain boundaries in the structure and allows electrons to move more easily within the crystal structure (Moazami et al. 2015). The average particle size of the synthesized $TiO_2$ nanopowders was calculated as 13.54 nm. This average particle size is consistent with the average particle sizes of $TiO_2$ used in high-performance DSSC applications (Akman et al. 2020; Huang et al. 2022; Richhariya et al. 2023).

Surface photographs of the synthesized $TiO_2$ were examined with FE-SEM. The SEM photograph given in Fig. 6 reflected close-contact spherical particles with an average diameter of 100 mn. Such close contact facilitates electron transport at the interface and allows greater dye absorption at the surface (Ge et al. 2021).

Figure 7 shows the EDS graphs of $TiO_2$ particles produced by the hydrothermal method. The presenceof titanium and oxygen in the structure is clearly understood from the EDS peaks.

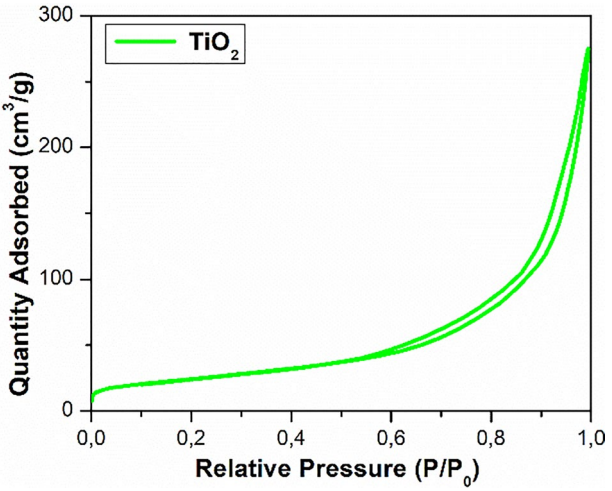



**Fig. 8** Plots showing the $N_2$ adsorption/desorption of generated $TiO_2$ nanoparticles

When it comes to redox cycles and dye loading of DSSCs, the surface area and porosity of $TiO_2$ nanopowders are crucial. We examined the pore size and specific surface area of the produced $TiO_2$ nanoparticles using the BET technique. The isotherm curve of $N_2$ gas based on the principle of adsorption and desorption was shown in Fig. 8. The generated $TiO_2$ nanoparticles demonstrated the presence of mesoporous structure and represented isotherm type IV by the Brunauere Deminge DemingeTeller (BDDT) classification (Xu et al. 2015). The produced $TiO_2$ particles were found to have a specific surface area of 6.36 $m^2/g$. The porosity of the $TiO_2$-based photoanode was determined by the BJH (Barret-Joyner-Halenda) method. The $TiO_2$ thin film's mean pore radius and pore volume were determined to be 61.95 nm and 0.189 $cm^3/g$, respectively. Large surface area and pore size photoanodes were known to enhance electrolyte transport pathways and dye loading in DSSCs (Wali et al. 2016). BET studies showed that the obtained parameters are suitable for high-performance DSSCs (Sayahi et al. 2021; Anitha et al. 2015).

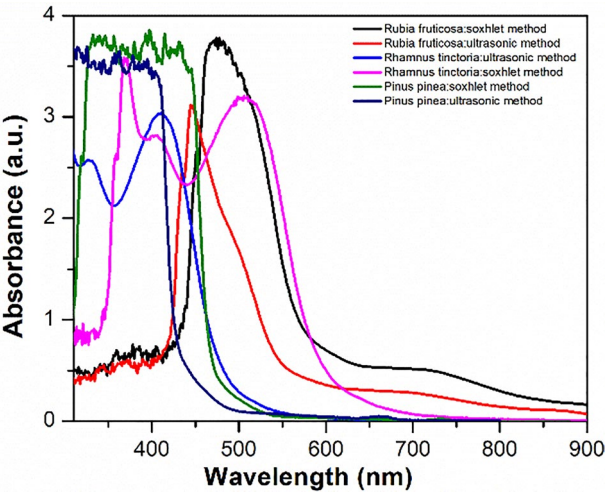



**Fig.9** UV–vis absorption spectra of extracted natural dyes

The absorption spectra of dyes extracted from *Pinus pinea* bark, *Rhamnus tinctoria* seeds, and *Rubia fruticosa* fruits by soxhlet and ultrasonic method were shown in Fig. 9. Dyes extracted from natural plants exhibited different absorption spectra. Variations and discrepancies in sensitizing dyes' absorption behavior were indicative of various pigment structures. Absorption spectra ranging from about 300 to 550 nm were detected in the dyes quercetin, emodin, and alizarin extracted from natural plants. Absorption bands in the near-UV–vis region (300–350 nm) reflect the $\pi-\pi^*$ transition, while bands in the visible blue region (about 450 nm) correspond to intramolecular charge transfer between donor–acceptor (Sen et al. 2023). Extraction methods led to differences in the maximum absorption wavelengths of the dyes. The maximum absorption wavelengths of the dyes extracted from the bark of the *Pinus pinea* plant by soxhlet and ultrasonic methods were observed at 397 nm and 361 nm, respectively. The peaks in the UV region of the dyes leached by two different methods indicate the presence of quercetin in the dyes. It can be said that the absorption of quercetin dye extracted by the Soxhlet method shifts towards the visible regiosn. The dyes extracted from the fruits of the *Rubia fruticosa* plant using soxhlet and ultrasonic methods had maximum absorption wavelengths of 445 and 476 mn, respectively. These observed peaks indicate the presence of alizarin pigment in the dyes. Additionally, Alizarin dye extracted by the Soxhlet method exhibited absorption in a wider wavelength range in the visible region, from 435 to 571 nm. The soxhlet method yielded two strong absorption peaks at 310 and 500 nm, while the ultrasonic method yielded peaks at 290 and 440 nm for the dye extracted from *Rahamnus tinctoria*. These peaks observed in the UV and visible regions confirm the presence of emodin pigment in the dye. In addition, emodin dye extracted by the soxhlet method exhibited absorption in a wider wavelength range (between 420–575 nm) in the visible region compared to other dyes. The presence of the pigments quercetin, alizarin and emodin in natural dyes was confirmed by the references to peaks made in previously reported studies (Prakash and Janarthanan 2023; Inbarajan et al. 2022; Kabir et al. 2022a). Here it seems that soxhlet is the best method to extract quercetin, alizarin and emodin pigments, because all dyes extracted by the soxhlet method showed stronsger absorption behavior. When six dyes made from real plants using two different processes were compared, the dye emodin that was leached from *Rhamnus tinctoria* seeds absorbed the biggest amount of light. This higher absorbance led to higher efficiency of emodin dye-sensitized DSSC leached by the soxhlet method. It is predicted that intense absorptions seen in the visible region improve cell performance (Safie et al. 2017). These absorptions in different energy regions helped the DSSC to capture photons and hence improve cell performance (Das et al. 2020). UV–vis absorptions of quercetin, emodin, and alizarin dyes extracted from natural plants were measured in this study, indicating that these dyes can be used as photoanode sensitizers.

Infrared (IR) spectroscopy application is used especially in the identification of organic molecules by considering certain functional groups (Thangavel et al. 2022). This spectroscopy helps to detect functional groups in dyes that play an active role in DSSCs. The Fourier transform infrared spectra (FTIR) of quercetin, emodin, and alizarin dyes extracted by different methods from *Pinus pinea* bark, *Rhamnus tinctoria* seeds, and *Rubia fruticosa* fruits, respectively, in the frequency range of 4000–400 $cm^{-1}$ are given in Fig. 10. Each spectrum displays the distinctive absorption bands that correlate with the chemical makeup of the dyes extracted using the soxhlet and ultrasonic methods, as shown in Fig. 10. The dyes leached by different extraction methods showed similar spectral properties among themselves, and the pigments (quercetin, emodin, and alizarin) in the structure confirmed the existence of their functional groups (Safaei-Ghomi et al. 2020; Akin et al. 2016; Xavier et al. 2021). The chemical structures of the extracted sensitizing dyes are given in Fig. 11.

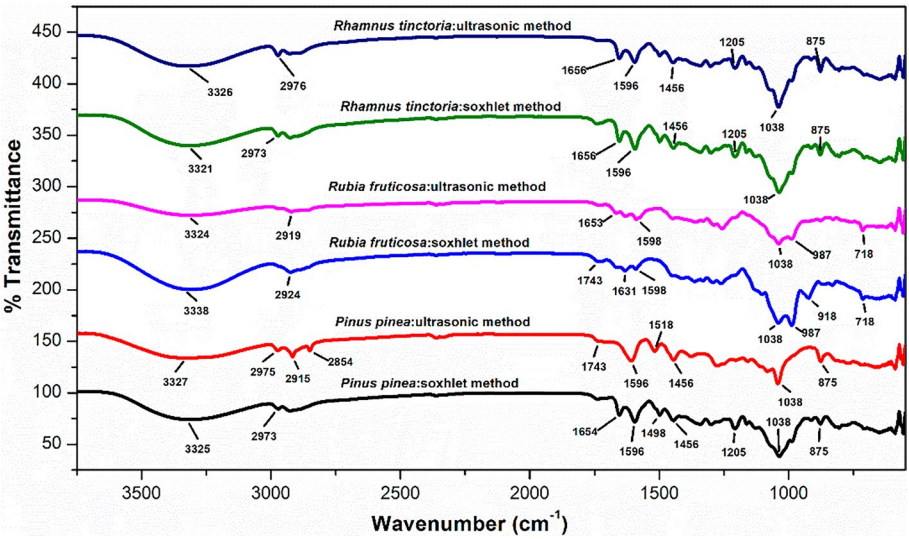



**Fig. 10** FTIR spectra of natural plant extracts

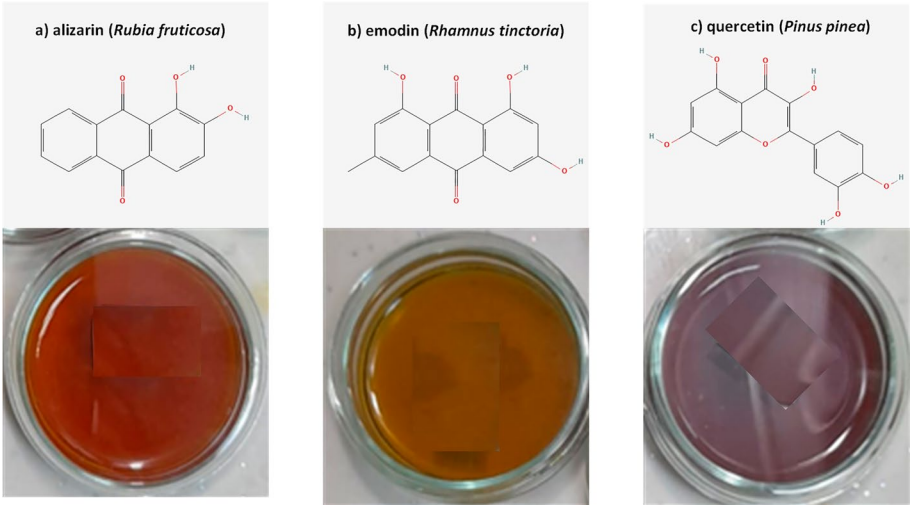



**Fig. 11** Chemical structures of alizarin (**a**), emodin (**b**), and quercetin dyes (**c**) extracted from different natural plants

Dye molecules can stick to the surface of the metal oxide layer through various binding mechanisms such as hydrogen bonding, covalent bonding, and Van-der Vaals forces (Zhang and Cole 2015). However, a strong interaction with $TiO_2$ surface atoms is only possible through covalent bonding. Because other interactions are weak and can make the device unstable. The strong interaction of the carbonyl and hydroxyl groups in natural dye molecules with the hydroxyl group on the surface of the porous photoanode ($TiO_2$) provides a better electron transfer to the conduction band of $TiO_2$. In other

words, these groups on the metal oxide surface increase the electron injection rate in cells (Subramanian and Wang 2012).

The O–H (hydroxyl) group is present in the extracts made using the two distinct extraction techniques, as shown by the wide bands between 3321 and 3338 $cm^{-1}$ (Rajan and Cindrella 2019). The asymmetric and symmetric vibrational modes corresponding to the C-H stretch vibrations are responsible for the peaks that appear between 2848 and 2976 $cm^{-1}$, indicating the presence of the aromatic C-H group (Ammar et al. 2019). The C = O stretching mode vibrations are thought to be responsible for the small shoulder peak that corresponds to a frequency of 1743 $cm^{-1}$ (Singh et al. 2021). Of > C = O, the stretching vibrational mode is represented by the peaks at 1656, 1653, and 1654 $cm^{-1}$ (Montagni et al. 2023). According to previous research (Güzel et al. 2018), vibrations of the aromatic ring and aromatic C = C bond are responsible for the peaks seen at 1596 and 1456 $cm^{-1}$, respectively. Strong bands seen at 1038 $cm^{-1}$ are caused by the C-O stretching vibrational modes, while the peak at 1205 $cm^{-1}$ is attributed to the amine groups' C-N bending (Safaei-Ghomi and R.* Masoomi, M. Hosseinpour, H. Batooli 2020). The bands at 987 and 918 $cm^{-1}$ are a result of out-of-plane bending of the C-H atom. Moreover, the planar bending vibration peaks of O–C–O are corresponding to the 718 and 875 $cm^{-1}$ peaks, respectively (Hajji et al. 2017). It is well known that functional groups in dye molecules, such as hydroxyl or/and carbonyl, can more effectively form bonds between the dye molecules and the $TiO_2$ surface. Better electron transfer to the $TiO_2$ conduction band is made possible by the strong interaction between the hydroxyl or/and carbonyl groups in natural dye molecules and the hydroxyl group on the $TiO_2$ surface (Singh et al. 2021). The functional groups in the sensitizing dyes affected the performance of the produced DSSCs. Compared to other dyes, the best sensitizer was obtained from *Rhamnus tinctoria* seeds by the soxhlet method ($\eta = 0.47$, $J_{sc} = 0.92$ mA/$cm^2$, FF = 0.72 and $V_{oc} = 0.71$ V). This could be because the dye extracted from *Rhamnus tinctoria* seeds contains hydroxyl groups, which can bind strongly to the $TiO_2$ surface (Safaei-Ghomi et al. 2020). In addition, the dye extracted from *Rubia fruticosa* by the soxhlet method exhibited better sensitizing properties than the dye extracted from *Rhamnus tinctoria* by the ultrasonic method. This showed that pigment diversity and extraction methods in plants may exhibit different sensitization performances. On the other hand, dyes extracted from *Pinus pinea* bark by two different methods showed low $V_{oc}$ (ultrasonic-0.36 V, soxhlet-0.41 V) and $J_{sc}$ (ultrasonic-0.06 mA/$cm^2$, soxhlet-0.11 mA/$cm^2$) values in DSSCs. The reason for this low $V_{oc}$ and $J_{sc}$ compared to other extracts may have been due to the low concentration of some functional groups that have high performance in DDSCs (Hamadanian et al. 2012). FTIR test results of dyes extracted from *Pinus pinea* bark, *Rhamnus tinctoria* seeds, and *Rubia fruticosa* fruits by different methods in this study showed that these natural pigments with carbonyl or/and hydroxyl groups can be used as suitable sensitizers in DSSCs.

Figure 12 shows the $J_{sc}$-V curves of DSSCs made with natural dyes, and Table 1 summarizes their photovoltaic parameters. Photovoltaic measurements were carried out under 100 mW/$cm^2$ illumination (AM 1.5G). Equation 2 and 3 were used to calculate the power conversion efficiency ($\eta$) and filling factor (FF) of the prepared DSSCs (Franchi et al. 2023). While $P_{max}$ and $P_{in}$ in these equations represent the maximum output power and input power, respectively, $V_{oc}$, FF and $J_{sc}$ correspond to the open circuit voltage, filling factor and short circuit current density. $J_{max}$ and $V_{max}$ reflect the maximum current density and maximum voltage, respectively.

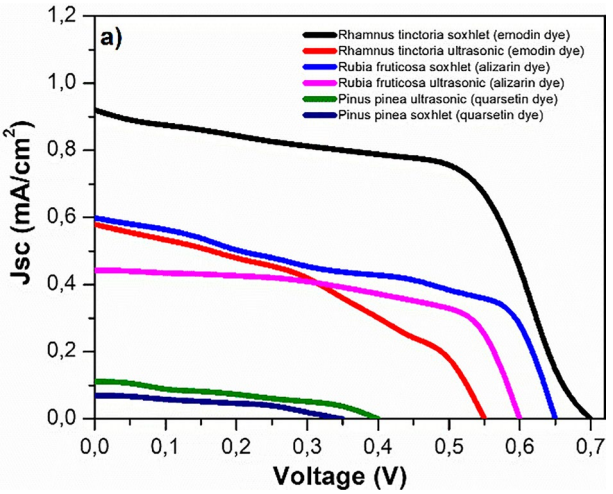



**Fig. 12** $J_{sc}$-V curves plots of DSSCs produced using different sensitizing dyes

**Table 1** Photovoltaic parameters of DSSCs made with various natural sensitizing dyes

| Sample | $J_{sc}$ (mA/cm$^2$) | $V_{oc}$ (V) | FF | $\eta$ (%) |
|---|---|---|---|---|
| *Rhamnus tinctoria*:soxhlet (emodin dye) based DSSC | 0.92 | 0.71 | 0.72 | 0.47 |
| *Rhamnus tinctoria*:ultrasonic (emodin dye) based DSSC | 0.57 | 0.56 | 0.65 | 0.20 |
| *Rubia fruticosa*:soxhlet (alizarin dye) based DSSC | 0.59 | 0.65 | 0.71 | 0.27 |
| *Rubia fruticosa*:ultrasonic (alizarin dye) based DSSC | 0.44 | 0.54 | 0.65 | 0.154 |
| *Pinus pinea*:soxhlet (quercetin dye) based DSSC | 0.11 | 0.41 | 0.63 | 0.028 |
| *Pinus pinea*:ultrasonic (quercetin dye) based DSSC | 0.06 | 0.36 | 0.62 | 0.013 |

$$\eta = \frac{P_{\max}}{P_{in}} = \frac{V_{oc} \times J_{sc} \times FF}{P_{in}} \tag{2}$$

$$FF = \frac{J_{\max} \times V_{\max}}{J_{sc} \times V_{oc}} \times 100 \tag{3}$$

The cell using the sensitizer extracted from *Rhamnus tinctoria* seeds by the soxhlet method showed the highest power conversion efficiency (0.47%) with $J_{sc}$ 0.92 mA/cm$^2$, $V_{oc}$ 0.71 V and FF 0.72. DSSCs using dyes leached by the Soxhlet method exhibited superior cell performance compared to the ultrasonic method. This can be explained by the fact that the dyes extracted by the Soxhlet method show absorption at a wider wavelength in the visible region and the high interaction of carbonyl or/and hydroxyl groups in the sensitizers with the $TiO_2$ surface provides a better charge transfer (Kabir et al. 2022b). The low power conversion efficiency of ultrasonically leached dyes in DSSCs may be due to the degradation of some high-performance functional groups during extraction. This situation restricts the dye's interaction with the $TiO_2$ surface (Hamadanian et al. 2012). Moreover, DSSCs using emodin and alizarin dyes extracted *from Rhamnus tinctoria* and *Rubia fruticosa* by the soxhlet method showed maximum $V_{oc}$ values of 0.71 and 0.65 V, respectively.

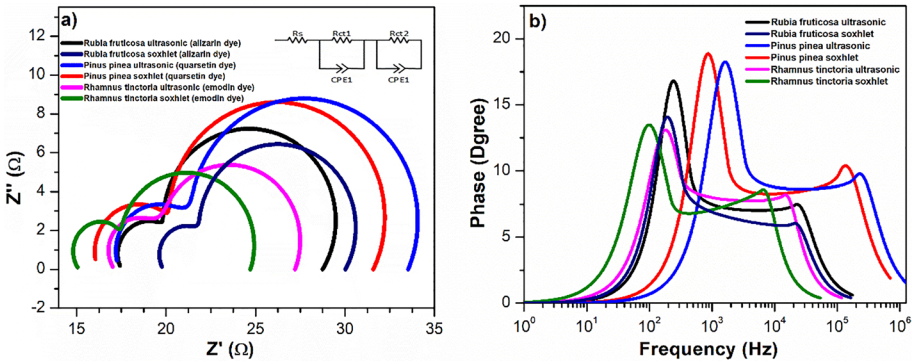



**Fig. 13** **a** Nyquist curves, **b** Bode plots of DSSCs produced using different sensitizing dyes

**Table 2** EIS parameters of DSSCs sensitized with various natural dyes

| Sample | $R_s$ (Ω) | $R_{ct1}$ (Ω) | $R_{ct2}$ (Ω) | $\tau_e(\mu s)$ |
|---|---|---|---|---|
| *Rhamnus tinctoria*:soxhlet (emodin dye) based DSSC | 15.6 | 5.3 | 105.7 | 1502 |
| *Rhamnus tinctoria*:ultrasonic (emodin dye) based DSSC | 16.8 | 8.4 | 167.7 | 784 |
| *Rubia fruticosa*:soxhlet (alizarin dye) based DSSC | 19.6 | 8.1 | 162.1 | 804 |
| *Rubia fruticosa*:ultrasonic (alizarin dye) based DSSC | 17.4 | 10.9 | 217.3 | 591 |
| *Pinus pinea*:soxhlet (quercetin dye) based DSSC | 16.4 | 43.9 | 869.2 | 171 |
| *Pinus pinea*:ultrasonic (quercetin dye) based DSSC | 17.1 | 80.5 | 1593.6 | 97 |

The high $V_{oc}$ values in DSSCs are due to the high interaction of the alkyl chains in the dye with the $TiO_2$ surface. Thanks to this strong steric barrier, electrons in the $TiO_2$ thin film were prevented from leaking into the electrolyte solution (Lin et al. 2015). On the other hand, it was determined that the photovoltaic parameters of DSSCs sensitized with quercetin dye extracted from *Pinus pinea* bark by soxhlet method were quite low, such as $V_{oc}$ 0.36 and $J_{sc}$ 0.06 mA/cm$^2$. These low $V_{oc}$ and $J_{sc}$ values seen in DSSCs may be due to the low concentration of some high-performance pigments and insufficient electron injection into the cells, respectively (Narayan 2012). FF has a significant impact on the performance of DSSCs. DSSCs sensitized with dyes using the ultrasonic method have a high recombination rate and, accordingly, they have lower FF values than cells sensitized with dyes using the soxhlet method, because low charge recombination indicates maximum photoelectron lifetime and minimum dark current. This allows the cell to have higher FF values (Tian et al. 2011; Yedidi et al. 2014). As a result, natural dyes obtained by different extraction methods may exhibit different sensitization performances. With sensitizers leached by various methods, photovoltaic parameters such as $V_{oc}$ and $J_{sc}$ can be improved in DSSCs. In addition, thanks to the practical applications of these methods, more economically suitable solar energy devices can be produced.

Interfacial charge transfer of DSSCs sensitized with natural dyes was investigated using electrochemical impedance spectroscopy (EIS). Under 100 mW/cm$^2$ light intensity, the response of the prepared cells to 10 mV open circuit voltage was measured in the frequency range from 0.1 Hz to 100 kHz. Figure 13a shows the Nyquist curves of various DSSCs

produced. Additionally, the resistance parameters calculated from the equivalent circuit are summarized in Table 2 using Zview software. The charge transfer resistance at the Pt/counter electrode/electrolyte interface is defined as the high-frequency region. The recombination resistance ($R_{ct2}$) at the $TiO_2$/sensitizing dye/electrolyte interface is reflected by larger semicircles in the mid-frequency region. The low-frequency region corresponds to the Warburg resistance and redox couple ($I^{-3}/I^{-}$) diffusion properties (Chandra Maurya et al. 2019). A Nyquist diagram typically has three semicircles, but in Fig. 13a only two semicircles are visible in the high and mid-frequency regions. The undetectable third semicircle may be due to Warburg diffusion of redox couples in the electrolyte or time constant difference (Bella et al. 2016). $R_s$ in Table 2 represents the series resistance, $R_{ct1}$ represents the electron transport resistance at the counter electrode, and $R_{ct2}$ represents the electron transfer resistance between $TiO_2$/electrolyte, which is directly proportional to the diameter of the arc at medium frequency. DSSCs sensitized with dyes extracted from natural plants by soxhlet and ultrasonic method showed charge transfer resistance ranging from 105.7 to 1593.6 Ω. It is understood from Table 2 that the plant variety and extraction methods significantly affected the load transfer resistance of the cells produced. Devices sensitized with quercetin dyes leached from the bark of the *Pinus pinea* plant by soxhlet and ultrasonic method showed high load transfer resistance. High charge transfer resistance indicated a higher rate of degradation and detachment, resulting in lower cell efficiency (Lohrasbi et al. 2013; Qi et al. 2018). In addition, as the $R_{ct2}$ value increased in the produced samples, it was observed that the $V_{oc}$ values decreased from 0.71 to 0.36. High $R_{ct2}$ values caused slower electron recombination between $TiO_2$/dye/redox, which negatively affects the $V_{oc}$ values (Rajan and Cindrella 2019). On the other hand, it was observed that DSSC sensitized with emodin dye extracted from *Rhamnus tinctoria* seeds by the soxhlet method had the lowest charge transfer resistance ($R_{ct2}=105.7$ Ω) and longer electron lifetime ($\tau_e=590$ $\mu s$). The lower $R_{ct2}$ and higher $\tau_e$ values observed in this cell are consistent with the higher power conversion efficiency ($\eta=0.47$) of this native dye-sensitized cell.

The Bode phase plot corresponding to the charge transfer process of cells sensitized with natural dyes is shown in Fig. 13b. In low-frequency regions, Bode curves are closely related to electron lifetime. Long electron lifetime reflects improved electron collection ability and low recombination resistance. The electron recombination lifetime ($\tau_e$) is calculated using Eq. 4 (Akman and Karapinar 2022); in this equation, $f_{max}$ is the Bode peak. The highest electron lifetime ($\tau_e=590$ µs) was observed in DSSC sensitized with emodin dye extracted from *Rhamnus tinctoria* seeds by the soxhlet method. In a study by Akman, it was emphasized that cells with a long electron lifetime limit the recombination of photo-injected electrons and redox pair $I^-/I^{3-}$ ions, thus leading to a significant improvement in the efficiency of DSSCs (Akman 2020). On the other hand, the $f_{max}$ of the cell sensitized with quercetin dye extracted from *Pinus pinea* barks by the ultrasonic method is in the high-frequency region; therefore, $\tau_e$ has the lowest value with 39.3 µs. The low $\tau_e$ value observed in this cell negatively affected the efficiency of this device ($\eta=0.013$). When Table 1 and 2 are examined, it is seen that electron lifetimes and photoelectrical parameters of DSSCs support each other.

$$\tau_e = \frac{1}{2\pi f_{(\max)}} \tag{4}$$

## 4 Conclusion

In this, natural dyes leached from *Rhamnus tinctoria* seeds, *Rubia fruticosa* fruits, and *Pinus pinea* bark by soxhlet and ultrasonic method were used as sensitizers in $TiO_2$-based DSSCs. FTIR spectra revealed the presence of functional groups found in natural dyes. It was concluded that natural pigments containing carbonyl or/and hydroxyl groups are good sensitizers for DSSCs. It was observed that the dyes extracted by various methods exhibited different absorption behaviors in the UV–vis region. Different extraction methods caused differences in the maximum absorption wavelengths of the dyes. Dyes extracted by the Soxhlet method showed absorption in a wider wavelength range in the UV–vis region. DSSC sensitized with dye extracted from *Rhamnus tinctoria* seeds by the soxhlet method showed the highest cell performance ($\eta = 0.47$). This situation was explained by the strong interaction of the carbonyl and/or hydroxyl groups in the emodin dye extracted by the Soxhlet method with the $TiO_2$ surface and the absorption behavior in a wider wavelength range in the visible region. It was also concluded that the resistance parameters obtained from EIS analyses and the photovoltaic parameters of the cells supported each other. It was understood that the DSSC with the highest power conversion efficiency ($\eta = 0.47$) had lower $R_{ct2}$ and higher $\tau_e$ value. Recent advances in DSSCs produced using different natural sensitizers have led to the use of dyes with high absorbency in the UV–vis region. The extraction method used to extract dyes has a major impact on the efficiency of DSSCs. Because natural dyes are inexpensive and environmentally friendly, using them in DSSCs is a good alternative. In addition, light harvesting natural dyes for DSSCs could provide a sustainable solution to meet future energy needs.

**Author Contributions** FA: Experimental studies, methodology, resources, scientific calculation, edits, research and writing the original draft.

**Funding** Open access funding provided by the Scientific and Technological Research Council of Türkiye (TÜBİTAK).

**Data availability** Not applicable for this study.

## Declarations

**Conflict of interest** In this study, the authors declare that they have no conflict of interest.

**Ethical approval** Not applicable for this study.

**Open Access** This article is licensed under a Creative Commons Attribution 4.0 International License, which permits use, sharing, adaptation, distribution and reproduction in any medium or format, as long as you give appropriate credit to the original author(s) and the source, provide a link to the Creative Commons licence, and indicate if changes were made. The images or other third party material in this article are included in the article's Creative Commons licence, unless indicated otherwise in a credit line to the material. If material is not included in the article's Creative Commons licence and your intended use is not permitted by statutory regulation or exceeds the permitted use, you will need to obtain permission directly from the copyright holder. To view a copy of this licence, visit http://creativecommons.org/licenses/by/4.0/.

## References


Agrícolas C., Veterinaria A.Y., Química C., Antioxidantes P., Fenólico Y.P., Corteza D.E.L.A., Pinus D.E.P., millenium, 2: 79–87.

Ahmad, P.A., Mir, F.A., Ullah, F., Bhat, M.A., Rather, M.H.: A study on fabrication and characterization of dye sensitized solar cells with carissa spinuram, iresine herbstii and ipomoea purpurea as sensitizers in visible light. Opt. Quant. Electron. **55**, 1–21 (2023). https://doi.org/10.1007/s11082-022-04129-1

Akin, S., Açikgöz, S., Gülen, M., Akyürek, C., Sönmezoğlu, S.: Investigation of the photoinduced electron injection processes for natural dye-sensitized solar cells: The impact of anchoring groups. RSC Adv. **6**, 85125–85134 (2016). https://doi.org/10.1039/c6ra19653e

Akman, E.: Enhanced photovoltaic performance and stability of dye-sensitized solar cells by utilizing manganese-doped ZnO photoanode with europium compact layer. J. Mol. Liq. **317**, 114223 (2020). https://doi.org/10.1016/j.molliq.2020.114223

Akman, E., Karapinar, H.S.: Electrochemically stable, cost-effective and facile produced selenium@activated carbon composite counter electrodes for dye-sensitized solar cells. Sol. Energy **234**, 368–376 (2022). https://doi.org/10.1016/j.solener.2022.02.011

Akman, E., Akin, S., Ozturk, T., Gulveren, B., Sonmezoglu, S.: Europium and terbium lanthanide ions co-doping in TiO2 photoanode to synchronously improve light-harvesting and open-circuit voltage for high-efficiency dye-sensitized solar cells. Sol. Energy **202**, 227–237 (2020). https://doi.org/10.1016/j.solener.2020.03.108

Alinejad, M., Buraidah, M.H., Teo, L.P., Arof, A.K.: Saffron dye-sensitized solar cells with polyvinyl alcohol based gel polymer electrolytes. Opt. Quant. Electron. **55**, 1–12 (2023). https://doi.org/10.1007/s11082-023-05078-z

Ammar, A.M., Mohamed, H.S.H., Yousef, M.M.K., Abdel-Hafez, G.M., Hassanien, A.S., Khalil, A.S.G.: Dye-sensitized solar cells (DSSCs) based on extracted natural dyes. J. Nanomater. (2019). https://doi.org/10.1155/2019/1867271

Anitha, V.C., Banerjee, A.N., Joo, S.W., Min, B.K.: Fabrication of hierarchical porous anodized titania nano-network with enhanced active surface area: Ruthenium-based dye adsorption studies for dye-sensitized solar cell (DSSC) application. J. Ind. Eng. Chem. **29**, 227–237 (2015). https://doi.org/10.1016/j.jiec.2015.03.032

Aslan, F.: Increasing the photoelectric conversion efficiency of dye-sensitized solar cells by doping SrAl2O4: Eu+2, Dy+3 to TiO2-based photoanodes. Phys. B **668**, 415267 (2023). https://doi.org/10.1016/j.physb.2023.415267

Bella, F., Galliano, S., Falco, M., Viscardi, G., Barolo, C., Grätzel, M., Gerbaldi, C.: Unveiling iodine-based electrolytes chemistry in aqueous dye-sensitized solar cells. Chem. Sci. **7**, 4880–4890 (2016). https://doi.org/10.1039/c6sc01145d

Calogero, G., Di Marco, G., Cazzanti, S., Caramori, S., Argazzi, R., Di Carlo, A., Bignozzi, C.A.: Efficient dye-sensitized solar cells using red turnip and purple wild Sicilian prickly pear fruits. Int. J. Mol. Sci. **11**, 254–267 (2010). https://doi.org/10.3390/ijms11010254

Calogero, G., Bartolotta, A., Di Marco, G., Di Carlo, A., Bonaccorso, F.: Vegetable-based dye-sensitized solar cells. Chem. Soc. Rev. **44**, 3244–3294 (2015). https://doi.org/10.1039/c4cs00309h

Calogero, G., Barichello, J., Citro, I., Mariani, P., Vesce, L., Bartolotta, A., Di Carlo, A., Di Marco, G.: Photoelectrochemical and spectrophotometric studies on dye-sensitized solar cells (DSCs) and stable modules (DSCMs) based on natural apocarotenoids pigments. Dyes Pigm. **155**, 75–83 (2018). https://doi.org/10.1016/j.dyepig.2018.03.021

Chandra Maurya, I., Singh, S., Srivastava, P., Maiti, B., Bahadur, L.: Natural dye extract from Cassia fistula and its application in dye-sensitized solar cell: experimental and density functional theory studies. Opt. Mater. **90**, 273–280 (2019). https://doi.org/10.1016/j.optmat.2019.02.037

Das, S.K., Ganguli, S., Kabir, H., Khandaker, J.I., Ahmed, F.: Performance of natural dyes in dye-sensitized solar cell as photosensitizer. Trans. Electr. Electron. Mater. **21**, 105–116 (2020). https://doi.org/10.1007/s42341-019-00158-y

Espinosa, N., Hösel, M., Angmo, D., Krebs, F.C.: Solar cells with one-day energy payback for the factories of the future. Energy Environ. Sci. **5**, 5117–5132 (2012). https://doi.org/10.1039/c1ee02728j

Franchi, D., Bartolini, M., D'Amico, F., Calamante, M., Zani, L., Reginato, G., Mordini, A., Dessì, A.: Exploring different designs in thieno[3,4-b]pyrazine-based dyes to enhance divergent optical properties in dye-sensitized solar cells. Processes. **11**, 3–16 (2023). https://doi.org/10.3390/pr11051542

Ge, Z., Wang, C., Chen, Z., Wang, T., Chen, T., Shi, R., Yu, S., Liu, J.: Investigation of the TiO2 nanoparticles aggregation with high light harvesting for high-efficiency dye-sensitized solar cells. Mater. Res. Bull. **135**, 111148 (2021). https://doi.org/10.1016/j.materresbull.2020.111148

Gómez-Ariza, J.L., Arias-Borrego, A., García-Barrera, T.: Multielemental fractionation in pine nuts (Pinus pinea) from different geographic origins by size-exclusion chromatography with UV and inductively coupled plasma mass spectrometry detection. J. Chromatogr. A **1121**, 191–199 (2006). https://doi.org/10.1016/j.chroma.2006.04.025

Güzel, E., Arslan, B.S., Durmaz, V., Cesur, M., Tutar, Ö.F., Sarı, T., İşleyen, M., Nebioğlu, M., Şişman, İ: Photovoltaic performance and photostability of anthocyanins, isoquinoline alkaloids and betalains as natural sensitizers for DSSCs. Sol. Energy **173**, 34–41 (2018). https://doi.org/10.1016/j.solener.2018.07.048

Hajji, S., Turki, T., Boubakri, A., Ben Amor, M., Mzoughi, N.: Study of cadmium adsorption onto calcite using full factorial experiment design. Desalinat. Water Treatment. **83**, 222–233 (2017). https://doi.org/10.5004/dwt.2017.21079

Hamadanian, M., Jabbari, V., Gravand, A., Asad, M.: Band gap engineering of TiO2 nanostructure-based dye solar cells (DSCs) fabricated via electrophoresis. Surf. Coat. Technol. **206**, 4531–4538 (2012). https://doi.org/10.1016/j.surfcoat.2012.03.017

Huang, Q., Wang, C., Shan, Q.: Quantitative deviation of nanocrystals using the RIR Method in x-ray diffraction (XRD). Nanomaterials **12**, 2320 (2022). https://doi.org/10.3390/nano12142320

Inbarajan, K., Sowmya, S., Janarthanan, B.: Direct and soxhlet extraction of dyes from the peels of Allium cepa and its effective application in dye–Sensitized solar cells as sensitizer. Opt. Mater. **129**, 112487 (2022). https://doi.org/10.1016/j.optmat.2022.112487

Kabir, F., Manir, S., Bhuiyan, M.M.H., Aftab, S., Ghanbari, H., Hasani, A., Fawzy, M., De Silva, G.L.T., Mohammadzadeh, M.R., Ahmadi, R., Abnavi, A., Askar, A.M., Adachi, M.M.: Instability of dye-sensitized solar cells using natural dyes and approaches to improving stability – an overview. Sustainable Energy Technol. Assess. **52**, 102196 (2022a). https://doi.org/10.1016/j.seta.2022.102196

Kabir, F., Bhuiyan, M.M.H., Hossain, M.R., Manir, M.S., Rahaman, M.S., Islam, M.T., Ullah, S.M.: Refining of red spinach extract for the enhanced photovoltaic performance of natural dye-based DSSC and degradation study. Optik **251**, 168452 (2022b). https://doi.org/10.1016/j.ijleo.2021.168452

Kocak, Y., Atli, A., Atilgan, A., Yildiz, A.: Extraction method dependent performance of bio-based dye-sensitized solar cells (DSSCs). Materials Research Express. **6**, 095512 (2019). https://doi.org/10.1088/2053-1591/ab2ef7

Kumar, B.A., Vetrivelan, V., Ramalingam, G., Manikandan, A., Viswanathan, S., Boomi, P., Ravi, G.: Computational studies and experimental fabrication of DSSC device assembly on 2D-layered TiO2 and MoS2@TiO2 nanomaterials. Phys. B Condensed Matter. **633**, 413770 (2022). https://doi.org/10.1016/j.physb.2022.413770

Lin, L., Peng, B., Shi, W., Guo, Y., Li, R.: Synthesis of zinc phthalocyanine with large steric hindrance and its photovoltaic performance for dye-sensitized solar cells. Dalton Trans. **44**, 5867–5874 (2015). https://doi.org/10.1039/c4dt03397c

Lohrasbi, M., Pattanapanishsawat, P., Isenberg, M., Chuang, S.S.C.: Degradation study of dye-sensitized solar cells by electrochemical impedance and FTIR spectroscopy, 2013 IEEE Energytech. Energytech **2013**, 1–4 (2013). https://doi.org/10.1109/EnergyTech.2013.6645304

Moazami, H.R., HosseinyDavarani, S.S., Mohammadi, J., Nojavan, S., Abrari, M.: The effect of electric field geometry on the performance of electromembrane extraction systems: footprints of a third driving force along with migration and diffusion. Analytica Chimica Acta. **891**, 151–159 (2015). https://doi.org/10.1016/j.aca.2015.06.030

Montagni, T., Rodríguez Chialanza, M., Cerdá, M.F.: Blueberries as a source of energy: physical chemistry characterization of their anthocyanins as dye-sensitized solar cells' sensitizers. Solar. **3**, 283–297 (2023). https://doi.org/10.3390/solar3020017

Mozaffari, S.A., Saeidi, M., Rahmanian, R.: Photoelectric characterization of fabricated dye-sensitized solar cell using dye extracted from red Siahkooti fruit as natural sensitizer, Spectrochimica Acta - part a: molecular and Biomolecular. Spectroscopy **142**, 226–231 (2015). https://doi.org/10.1016/j.saa.2015.02.003

Mphande, B.C.: Impact of extraction methods upon light absorbance of natural organic dyes for dye sensitized solar cells application. J. Energy Natural Resour. **3**, 38 (2014). https://doi.org/10.11648/j.jenr.20140303.13

Narayan, M.R.: Review: dye sensitized solar cells based on natural photosensitizers. Renew. Sustain. Energy Rev. **16**, 208–215 (2012). https://doi.org/10.1016/j.rser.2011.07.148

Nguyen, D.T., Kurokawa, Y., Taguchi, K.: Enhancing DSSC photoanode performance by using Ni-doped TiO2 to fabricate scattering layers. J. Electron. Mater. **49**, 2578–2583 (2020). https://doi.org/10.1007/s11664-020-07965-7

Nnorom, O.O., Onuegbu, G.C., Etus, C.: Photo-performance characteristics of Baphia nitida and rosella dye sensitized solar cell. Results Opt. **9**, 100311 (2022). https://doi.org/10.1016/j.rio.2022.100311

Obi, K., Frolova, L., Fuierer, P.: Preparation and performance of prickly pear (Opuntia phaeacantha) and mulberry (Morus rubra) dye-sensitized solar cells. Sol. Energy **208**, 312–320 (2020). https://doi.org/10.1016/j.solener.2020.08.006

Prabavathy, N., Balasundaraprabhu, R., Kristoffersen, A.S., Balaji, G., Prasanna, S., Sivakumaran, K., Kannan, M.D., Erga, S.R., Velauthapillai, D.: Enhanced photostability of anthocyanin dye for increased efficiency in natural dye sensitized solar cells. Optik. **227**, 166053 (2021). https://doi.org/10.1016/j.ijleo.2020.166053

Peiris, D.S.U., Ekanayake, P., Karunaratne, B.A., Petra, M.I.: Improved performance of DSSC photoanodes after the modification of TiO2 with reduced graphene oxide. J. Electron. Mater. **50**, 1044–1053 (2021). https://doi.org/10.1007/s11664-020-08642-5

Prakash, P., Janarthanan, B.: Review on the progress of light harvesting natural pigments as DSSC sensitizers with high potency. Inorg. Chem. Commun. **152**, 110638 (2023). https://doi.org/10.1016/j.inoche.2023.110638

Prakash, P., Ruba, N., Sowmya, S., Janarthanan, B.: A novel approach to dye-sensitized solar cells using natural cocktail photosensitizers with nano TiO2 semiconductor. Opt. Quant. Electron. **54**, 1–16 (2022). https://doi.org/10.1007/s11082-022-04242-1

Qi, K., Yuan Liu, S., Chen, Y., Xia, B., Li, G.D.: A simple post-treatment with urea solution to enhance the photoelectric conversion efficiency for TiO2 dye-sensitized solar cells. Solar Energy Mater. Solar Cells **183**, 193–199 (2018). https://doi.org/10.1016/j.solmat.2018.03.038

Rahman, S., Haleem, A., Siddiq, M., Hussain, M.K., Qamar, S., Hameed, S., Waris, M.: Research on dye sensitized solar cells: recent advancement toward the various constituents of dye sensitized solar cells for efficiency enhancement and future prospects. RSC Adv. **13**, 19508–19529 (2023). https://doi.org/10.1039/d3ra00903c

Rajan, A.K., Cindrella, L.: Studies on new natural dye sensitizers from Indigofera tinctoria in dye-sensitized solar cells. Opt. Mater. **88**, 39–47 (2019). https://doi.org/10.1016/j.optmat.2018.11.016

Rajkumar, S., Venkatraman, M.R., Balraju, P., Suguna, K., Pugazhendhi, A.: Performance of simple green synthesized Ag incorporated TiO2 nanoparticles based photoanodes by doctor-blade coating as working electrodes for dye sensitized solar cells. Prog. Org. Coat. **164**, 106697 (2022). https://doi.org/10.1016/j.porgcoat.2021.106697

Rajkumar, S., Nirmal Kumar, M., Suguna, K., Muthulakshmi, S., Kumar, R.A.: Enhanced performance of dye-sensitized solar cells using natural cocktail dye as sensitizer. Optik. **178**, 224–230 (2019). https://doi.org/10.1016/j.ijleo.2018.10.004

Ramamoorthy, R., Radha, N., Maheswari, G., Anandan, S., Manoharan, S., Victor, R.: Williams, Betalain and anthocyanin dye-sensitized solar cells. J. Appl. Electrochem. **46**, 929–941 (2016). https://doi.org/10.1007/s10800-016-0974-9

Ramirez-Perez, J., Maria, C., Santacruz, C.P.: Impact of solvents on the extraction and purification of vegetable dyes onto the efficiency for dye-sensitized solar cells. Renew. Wind Water Solar. **6**, 1–15 (2019). https://doi.org/10.1186/s40807-019-0055-x

Richhariya, G., Meikap, B.C., Kumar, A.: Review on fabrication methodologies and its impacts on performance of dye-sensitized solar cells. Environ. Sci. Pollut. Res. **29**, 15233–15251 (2022). https://doi.org/10.1007/s11356-021-18049-2

Richhariya, G., Kumar, A., Shukla, A.K., Shukla, K.N., Chanakaewsomboon, I.: Efficient photosensitive light harvesting dye sensitized solar cell using hibiscus and rhodamine dyes. J. Power Sources **572**, 233112 (2023). https://doi.org/10.1016/j.jpowsour.2023.233112

Safaei-Ghomi, J., Masoomi, R., Hosseinpour, M., Batooli, H.: Energy production using dye-sensitized solar cells by TiO 2 nanoparticles fabricated with several natural dyes. J Nanostruct. **10**, 691–701 (2020). https://doi.org/10.22052/JNS.2020.04.002

Safie, N.E., Ludin, N.A., Hamid, N.H., Tahir, P.M., Teridi, M.A.M., Sepeai, S., Ibrahim, M.A., Sopian, K.: Electron transport studies of dye-sensitized solar cells based on natural sensitizer extracted from rengas (Gluta spp.) and mengkulang (Heritiera elata) wood. BioResources. **12**, 9227–9243 (2017). https://doi.org/10.15376/biores.12.4.9227-9243

Sánchez-García, M.A., Bokhimi, X., Velázquez Martínez, S., Jiménez-González, A.E.: Dye-sensitized solar cells prepared with Mexican pre-hispanic dyes. J. Nanotechnol. **2018**, 1–8 (2018). https://doi.org/10.1155/2018/1236878

Sayahi, H., Aghapoor, K., Mohsenzadeh, F., MohebiMorad, M., Darabi, H.R.: TiO2 nanorods integrated with titania nanoparticles: Large specific surface area 1D nanostructures for improved efficiency of dye-sensitized solar cells (DSSCs). Solar Energy. **215**, 311–320 (2021). https://doi.org/10.1016/j.solener.2020.12.060

Sen, A., Putra, M.H., Biswas, A.K., Behera, A.K., Grob, A.: Insight on the choice of sensitizers/dyes for dye sensitized solar cells: a review. Dyes Pigments. **213**, 111087 (2023). https://doi.org/10.1016/j.dyepig.2023.111087

Senthamarai, R., Madurai Ramakrishnan, V., Palanisamy, B., Kulandhaivel, S.: Synthesis of TiO2 nanostructures by green approach as photoanodes for dye-sensitized solar cells. Int. J. Energy Res. **45**, 3089–3096 (2021). https://doi.org/10.1002/er.6002

Senthamarai, R., Madurai Ramakrishnan, V., Murugan, P., PonnusamyMunusamy, A., Kulandhaivel, S.: Synthesis and characterization of nickel doped TiO2 nanoparticles by green method and its performance as dye-sensitized solar cells photoanodes. Int. J. Energy Res. **46**, 7749–7757 (2022). https://doi.org/10.1002/er.7677

Sethy, P.P., Pani, T.K., Rout, S.: Structural and magnetic properties of Ni/C core–shell nanofibers prepared by one step co-axial electrospinning method. J. Mater. Sci. Mater. Electron. **807**, 1–15 (2023). https://doi.org/10.1007/s10854-023-10194-3

Shalini, S., BalasundaraPrabhu, R., Prasanna, S., Mallick, T.K., Senthilarasu, S.: Review on natural dye sensitized solar cells: operation, materials and methods. Renew. Sustain. Energy Rev. **51**, 1306–1325 (2015). https://doi.org/10.1016/j.rser.2015.07.052

Singh, S., Maurya, I.C., Sharma, S., Kushwaha, S.P.S., Srivastava, P., Bahadur, L.: Application of new natural dyes extracted from Nasturtium flowers (Tropaeolum majus) as photosensitizer in dye-sensitized solar cells. Optik **243**, 167331 (2021). https://doi.org/10.1016/j.ijleo.2021.167331

Sönmezolu, S., Akyürek, C., Akin, S.: High-efficiency dye-sensitized solar cells using ferrocene-based electrolytes and natural photosensitizers. J. Phys. D Appl. Phys. **45**, 425101 (2012). https://doi.org/10.1088/0022-3727/45/42/425101

Subramanian, A., Wang, H.W.: Effect of hydroxyl group attachment on TiO 2 films for dye-sensitized solar cells. Appl. Surf. Sci. **258**, 7833–7838 (2012). https://doi.org/10.1016/j.apsusc.2012.04.069

Tabacchi, G., Fabbiani, M., Mino, L., Martra, G., Fois, E.: The case of formic acid on anatase TiO2(101): where is the acid proton? Angew. Chem. Int. Edn. **58**, 12431–12434 (2019). https://doi.org/10.1002/anie.201906709

Teja, A.S., Srivastava, A., Satrughna, J.A.K., Tiwari, M.K., Kanwade, A., Chand Yadav, S., Shirage, P.M.: Optimal processing methodology for futuristic natural dye-sensitized solar cells and novel applications. Dyes Pigments. **210**, 110997 (2023). https://doi.org/10.1016/j.dyepig.2022.110997

Thangavel, S., Kathiravan, V., Ashok Kumar, R., Satheesh Kumar, G., Selvarajan, P.: Spectral, optical, mechanical, impedance, and nonlinear optical properties of amaranth (dye)-doped l-histidine hydrochloride monohydrate crystal. J. Mater. Sci. Mater. Electron. **33**, 12249–12258 (2022). https://doi.org/10.1007/s10854-022-08184-y

Tian, Y., Hu, C., Wu, Q., Wu, X., Li, X., Hashim, M.: Investigation of the fill factor of dye-sensitized solar cell based on ZnO nanowire arrays. Appl. Surf. Sci. **258**, 321–326 (2011). https://doi.org/10.1016/j.apsusc.2011.08.058

Vieito, C., Fernandes, É., Velho, M.V., Pires, P.: The effect of different solvents on extraction yield, total phenolic content and antioxidant activity of extracts from pine bark (Pinus pinaster subsp. atlantica). Chem. Eng. Trans. **64**, 127–132 (2018). https://doi.org/10.3303/CET1864022

Wali, Q., Bakr, Z.H., Manshor, N.A., Fakharuddin, A., Jose, R.: Science Direct SnO2–TiO2 hybrid nanofibers for efficient dye-sensitized solar cells. Solar Energy **132**, 395–404 (2016). https://doi.org/10.1016/j.solener.2016.03.037

Wang, X.F., Matsuda, A., Koyama, Y., Nagae, H., İchi Sasaki, S., Tamiaki, H., Wada, Y.: Effects of plant carotenoid spacers on the performance of a dye-sensitized solar cell using a chlorophyll derivative: Enhancement of photocurrent determined by one electron-oxidation potential of each carotenoid. Chem. Phys. Lett. **423**, 470–475 (2006). https://doi.org/10.1016/j.cplett.2006.04.008

Weldekidan, H., Strezov, V., Town, G.: Review of solar energy for biofuel extraction. Renew. Sustain. Energy Rev. **88**, 184–192 (2018). https://doi.org/10.1016/j.rser.2018.02.027

Xavier, L., Barrenengoa, M., Dieste, A., Amilivia, A., Palombo, V., Sabag, M., Zecchi, B.: Valorization of Pinus taeda bark: source of phenolic compounds, tannins and fuel: characterization, extraction conditions and kinetic modelling. Europ. J. Wood Wood Prod. **79**, 1067–1085 (2021). https://doi.org/10.1007/s00107-021-01703-4

Xu, J., Wang, G., Fan, J., Liu, B., Cao, S., Yu, J.: G-C3N4 modified TiO2 nanosheets with enhanced photoelectric conversion efficiency in dye-sensitized solar cells. J. Power Sources **274**, 77–84 (2015). https://doi.org/10.1016/j.jpowsour.2014.10.033

Yedidi K., Tatapudi S., Mallineni J., Knisely B., Kutiche J., Tamizhmani G.: Failure and degradation modes and rates of PV modules in a hot-dry climate: results after 16 years of field exposure. In: 2014 IEEE 40th Photovoltaic Specialist Conference (PVSC). pp 3245–3247. doi https://doi.org/10.1109/PVSC.2014.6925626.

Yeoh, M.E., Chan, K.Y., Wong, H.Y., Low, P.L., How Thien, G.S., Ng, Z.N., Ananda Murthy, H.C., Balachandran, R.: Hydrothermal duration effect on the self-assembled $TiO_2$ photo-anode for DSSC application. Opt. Mater. **141**, 113907 (2023). https://doi.org/10.1016/j.optmat.2023.113907

Zatirostami, A.: Electro-deposited SnSe on ITO: A low-cost and high-performance counter electrode for DSSCs. J. Alloy. Compd. **844**, 156151 (2020). https://doi.org/10.1016/j.jallcom.2020.156151

Zatirostami, A.: A dramatic improvement in the efficiency of TiO2-based DSSCs by simultaneous incorporation of Cu and Se into its lattice. Opt. Mater. **117**, 111110 (2021). https://doi.org/10.1016/j.optmat.2021.111110

Zhang, L., Cole, J.M.: Anchoring groups for dye-sensitized solar cells. ACS Appl. Mater. Interfaces. **7**, 3427–3455 (2015). https://doi.org/10.1021/am507334m

**Publisher's Note** Springer Nature remains neutral with regard to jurisdictional claims in published maps and institutional affiliations.